

A Versatile Partial Sheet Cavitation Model

Surasak Phoemsapthawee¹, Jean-Baptiste Leroux¹, Jean-Marc Laurens¹, François Deniset²

¹Laboratoire Brestois des Mécaniques et des Systèmes (LBMS) - EA4325, ENSIETA, Brest, France

²Institut de Recherche de l'Ecole Navale (IRENav) - EA3634, Ecole Naval, Brest, France

ABSTRACT

This paper presents a partial sheet cavitation model and its validation. The partial sheet cavitation model has been developed and implemented within an unsteady potential flow code. However, as proposed in the model, there exists a relationship between the sheet cavitation geometry and the pressure distribution in non-cavitating condition, so the model can be implemented in various flow solvers. The objective of this study is to develop a fast numerical tool to access the hydrodynamic forces and performance of rudders and marine propellers with partial sheet cavitation effects in unsteady state flow conditions. The model has been first validated by comparing its results with experimental measurements on a 2D hydrofoil. A second stage of validation has been performed using some available measurements results of cavity length over a 3D hydrofoil. Finally, a series of experiments have been setup and performed in the cavitation tunnel of the BSHC to measure the hydrodynamic forces over a 3D cavitating hydrofoil. This last stage completes the model validation in steady state flow condition. Finally, results obtained by simulations in unsteady flow condition will also be presented and discussed.

Keywords

Sheet cavitation, Unsteady, Hydrostatic pressure, Hydrodynamic force, Vibration.

1 INTRODUCTION

The sheet cavitation affects the hydrodynamics forces of lifting bodies. The work of Balhan (1951) demonstrates that the lift coefficients C_L and the drag coefficients C_D of Kármán-Trefftz profiles vary with the cavitation number σ_V . When the cavitation number decreases, the lift coefficient slightly increases first and then collapses when the cavitation number is such that the cavity does not close on the foil surface. An example of the cavitation effect extracted from Balhan (1951) is presented in figure 1. It is generally admitted that the lift coefficient increases in presence of partial sheet cavitation and decreases abruptly when supercavitation occurs. Carlton (2007) uses these experimental data in the chapter 9 "Cavitation" of his book. To model the sheet cavitation, the understanding of this phenomenon is required. However, the mechanism of the

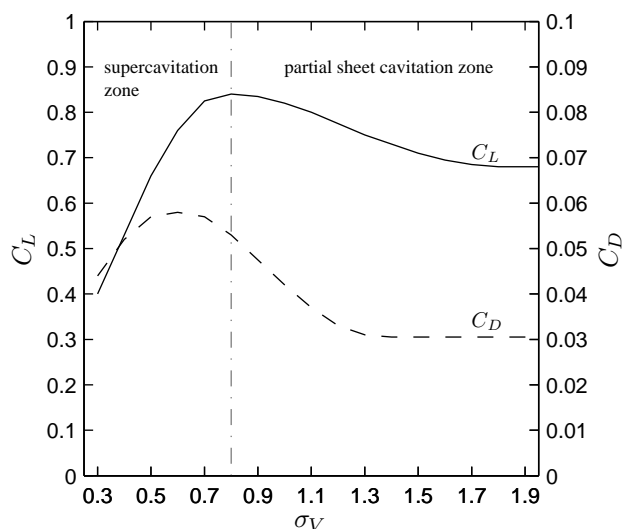


Figure 1: Effect of cavitation on the lift and drag coefficient of a Kármán-Trefftz profile; extracted from Balhan (1951)

sheet cavitation phenomenon is not yet completely understood. One important point in the phenomenon is how the cavity establishes over lifting bodies with round leading edge. Unlike downstream sharp-corner bodies, the mechanism is not completely understood. Franc (1986), stipulates from experimental observations that the leading-edge sheet cavitation requires a laminar-boundary-layer separation and the cavity establishes downstream of the laminar-boundary-layer separation point. This mechanism is widely accepted and used as the cavity detachment criterion for many sheet cavitation simulations; see for instance Briançon-Marjolet and Merle (1999); Salvator and Esposito (2001); Brewer and Kinnas (1997).

Nevertheless, Farhat et al. (2002) demonstrate that the sheet cavitation can occur with another mechanism. According to the experimental results obtained at the "Laboratoire de Machines Hydrauliques, Ecole Polytechnique Fédérale de Lausanne", the sheet cavitation phenomenon has been observed without any sign of laminar-boundary-layer separation. This observation might support the Brillouin-Villat criterion or the smooth detachment criterion. This criterion, consisting in choosing the point which guarantees the curvature continuity while respecting the slippery condi-

tion and the steam pressure, is used by most simulations, see for instance Kinnas and Fine (1993); Lee and Kinnas (2004).

Another important point is the cavity closure mechanism. As the cavity can collapse into bubbles or cloud cavitation, some simulations use the Rayleigh's bubble collapse equation as the cavity closure model (Yamaguchi and Kato, 1983). Nevertheless, the cavity can also close with a re-entrant jet mechanism. Krishnaswamy et al. (2001) and Vaz et al. (2003) simulate this mechanism over 2D hydrofoils with the potential flow theory.

The cavity closure models used in potential flow simulations can be classified in two categories: open and close models. Rowe and Blottiaux (1993) has given the definition that a close model is a model in which the streamline returns and touches the foil surface after having been deviated by the cavity, while an open model is a model in which the streamline does not retouch the foil surface after having been deviated by the cavity.

Most partial sheet cavitation simulations use the closed model for their cavity closure model (Kinnas and Fine, 1993; Briançon-Marjolet and Merle, 1999; Salvator and Esposito, 2001; Peallat and Pellone, 1996). Although the details of each model are different, the principle of the closed models is to transform in a continuous manner the vapor pressure dynamic condition on cavity surface into a zero normal velocity condition on the wet surface.

In most potential flow sheet cavitation simulations, see for instance Kinnas and Fine (1993); Salvator and Esposito (2001); Vaz et al. (2003), over the cavity planform, the dipole strengths distribution is imposed using the vapor pressure dynamic condition. The source strengths distribution which describes the cavity thickness distribution is the unknown to be determined. Yet, an iterative procedure is required to determine the cavity planform. Unlike those simulations, as a classic second generation potential flow code (Hoeijmakers, 1992), our unsteady 3D potential flow code imposes the source strengths distribution and determine the dipole strengths distribution. Our cavitation model imposes directly the cavity planform from the non-cavitating pressure distribution. In spite of that, an iterative procedure is still needed to determine the cavity thickness. In the same manner as in boundary layer simulation (Laurens, 1993), our cavitation model uses transpiration velocities v^* in order to simulate the sheet cavitation effect in the unsteady potential flow. However, as the model proposes a relationship between the sheet cavitation geometry and the pressure distribution in non-cavitating condition, this cavitation model can be used in another type of calculation code.

In the first stage of validation, the cavitation model is implemented within the 2D potential flow code developed and used within the framework of Leroux (2003). The pressure coefficient distribution of a 2D hydrofoil is computed and

compared with the experimental data presented in Leroux (2003) and Leroux et al. (2003). Then a second stage of validation is reached by simulating a 3D cavitating elliptic hydrofoil. The model is implemented within the potential flow code mentioned above. The computed cavity lengths are compared with measured cavity lengths from Kinnas and Fine (1993). The details of the first and the second stage validations were presented in Phoemsapthawee et al. (2008a). However, after an improvement of the implementation in the 3D potential flow code, the numerical results in the second stage are slightly modified and presented in Phoemsapthawee et al. (2008b).

As the objective of this development is to be able to estimate the effect of sheet cavitation over the hydrodynamic forces, a validation on hydrodynamic forces is required. In this paper, the final stage of validation in steady state flow condition is presented. An experiment has been conducted in the cavitation tunnel of the Bulgarian Ship Hydrodynamic Centre (BSHC). The lift and drag coefficients of a partially cavitating 3D hydrofoil have been measured to compare with our numerical simulations.

Finally, simulations of cavitating propeller working under a hydrostatic pressure field are also presented and discussed in order to study the performance of the cavitation model in unsteady state flow condition.

2 CAVITATION MODEL PRESENTATION

The partial sheet cavitation model is based on the existing relationship between the cavity geometry and the pressure distribution in non-cavitating condition. Equation 1 describes the proposed relationship between the non-dimension transpiration velocity \tilde{v}^* and the pressure coefficient distribution C_P . The non-dimension cavity thickness \tilde{t}_c , in other words the cavity geometry, is directly associated with the transpiration velocity as shown in equation 2.

$$\tilde{v}^* = -k \int_{\tilde{s}_0}^{\tilde{s}} (C_P + \sigma_V) d\tilde{s} \quad (1)$$

$$\tilde{t}_c = \frac{1}{\tilde{u}_c} \int_{\tilde{s}_0}^{\tilde{s}} \tilde{v}^* d\tilde{s} \quad ; \quad \tilde{t}_c \geq 0 \quad (2)$$

where \tilde{s} is the non-dimension curvilinear location and \tilde{s}_0 is the non-dimension cavity detachment location.

The non-dimension tangential velocity \tilde{u}_c over the cavity planform in equation 2 is assumed to be constant and associated with the vapor pressure or the cavitation number σ_V . By using the classical Bernoulli's equation, this \tilde{u}_c can be defined as shown in equation 3.

$$\tilde{u}_c = \sqrt{1 + \sigma_V} \quad (3)$$

The computation scheme is described here. Starting from the stagnation point and following the streamline, as long as the non-cavitating pressure is greater than the vapor

pressure ($C_P > -\sigma_V$), the transpiration velocity is set to zero since the cavity thickness can not have a negative value. The cavity detaches where the non-cavitating pressure passes the vapor pressure ($C_P = -\sigma_V$). This corresponds to the Brillouin-Villat criterion or the smooth detachment criterion. Then, the transpiration velocity as well as the cavity thickness is calculated using equations 1 and 2 until the cavity thickness \tilde{t}_c returns to zero. This way, the cavity planform depends only on the pressure coefficient distribution and on the cavitation number. No additional cavity closure model is required. However, an iterative procedure is needed to determine the adaptive factor k in equation 1. The secant method is applied; the criterion is to obtain the vapor pressure ($C_P = -\sigma_V$) at the maximum cavity thickness location.

As the model is defined on a streamline, an assumption is needed for the 3D simulations. It is assumed that the perturbation velocities are small compared to the upstream velocities. This assumption allows the implementation of the cavitation model in each band (section) of the lifting body.

In addition, for the unsteady state flow simulations, another assumption is required. Forced by the principle of the model, it is needed to assume that the vapor inertia due to phase change is negligible compared to the non-cavitating pressure fluctuation. Hence the cavity does not depend on the previous time-step cavity shape.

3 CAVITATION MODEL VALIDATION

As described in the introduction, the cavitation model has been validated with measured pressure coefficients over a 2D hydrofoil (Leroux, 2003) and with measured cavity lengths over a 3D hydrofoil (Kinnas and Fine, 1993). The detail of these comparisons are already presented in Phoemsapthawee et al. (2008a) and Phoemsapthawee et al. (2008b). Figure 2 presents the pressure coefficient distribution measured and computed for a 2D cavitating foil.

Now the final stage of the validation is presented. An experiment in cooperation with the Bulgarian Ship Hydrodynamic Centre (BSHC) has been performed. The detailed complete investigation of the experimental data as well as the proper numerical simulations will be the object of a joined publication with BSHC. Nevertheless, the first comparison results are presented here. A 3D hydrofoil with NACA0010 section is installed in the BSHC cavitation tunnel with a force transducer system. The hydrofoil is attached to the upper tunnel wall. A strut with the same section is installed between the hydrofoil and the tunnel wall so as to take the hydrofoil out of the tunnel wall boundary layer. The angle of attack of the strut is always set to zero. Only the forces over the hydrofoil are measured. The dimension of the hydrofoil, the strut and the tunnel section is presented in figure 3.

In the simulations, the upper-tunnel-wall effect is taken into account by applying the image theory and the other tunnel

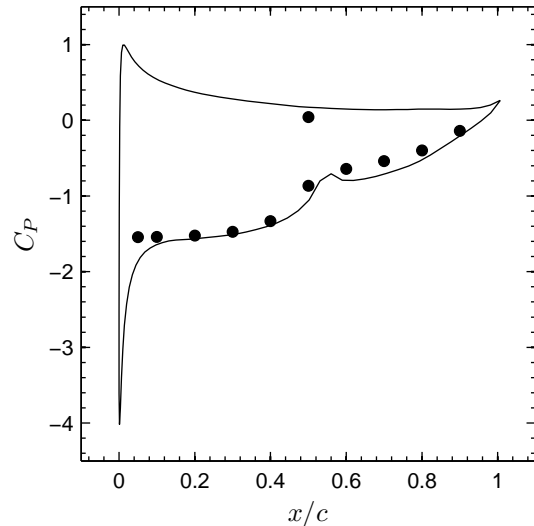


Figure 2: Comparison between the computed (—) and the measured (●) pressure coefficients over a 2D hydrofoil, section NACA66(mod)-312 $a=0.8$, $\alpha = 6^\circ$, $Re = 0.75 \times 10^6$, $\sigma_V = 1.495$

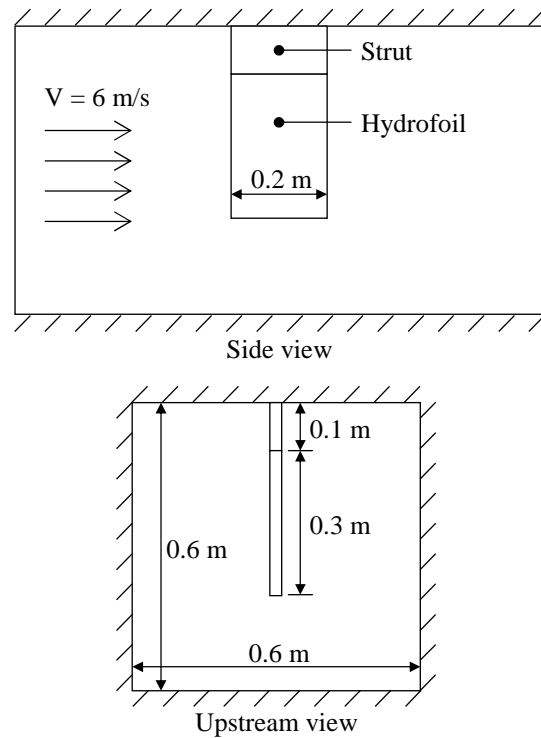


Figure 3: Configuration of the experiment performed in the BSHC cavitation tunnel

walls are represented by flat plates carrying dipoles distribution. The numerical model and meshes of the hydrofoil, the strut and the tunnel wall is presented in figure 4. No boundary layers effects are taken into account.

The angle of attack in the experiment is set to 7 degrees ($\alpha = 7^\circ$). However, from the difference of measured lift coefficients between the 7 and -7 degrees angle of attack in

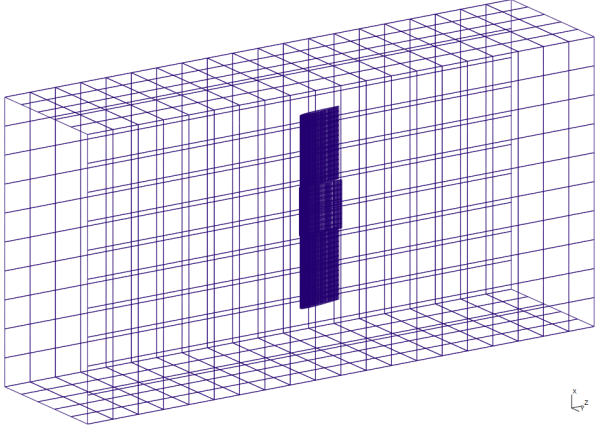


Figure 4: Meshes (without wake panels) used in the numerical simulation

non-cavitating condition, it is possible to have an error of 0.22 degrees or greater. The angle of attack in the numerical simulation is corrected to 7.22 degrees in order to better approach the experimental setup.

The comparison results in non-cavitating condition are shown in the table 1. The computed drag coefficients are a lot lower than the measured drag coefficients. This is usual for a potential flow simulation in which the viscosity effect is not taken into account. It is rather surprising that the computed lift coefficient is smaller than the measured lift coefficient. Nevertheless, the difference in lift coefficient comparison is lesser than 6%. This error might be due to the uncertainty in force measurement and/or in the error of velocity measurement.

Table 1: Comparison of lift and drag coefficients in non-cavitating condition of the 3D hydrofoil, section NACA0010, $\alpha = 7^\circ$

	C_L	C_D
Experiment	0.355	0.025
Simulation	0.335	0.015

Figure 5 (a) and (b) shows the comparison results of lift and drag coefficients in cavitating condition. The numerical results have the same tendency as the experimental results. The experimental results as well as the numerical results confirm that in case of partial sheet cavitation the lift and drag coefficients increase when the cavitation number decreases. Although we gain a little in lift coefficient with the presence of the partial sheet cavitation, the loss is more significant in lift-to-drag ratio ε_F as shown in figure 5 (c). The loss in lift-to-drag ratio between the numerical and the experimental results are comparable.

4 MARINE PROPELLER SIMULATIONS

In this section, numerical simulations have been performed in order to investigate the effect of partial sheet cavitation on the propeller performance both in steady and in un-

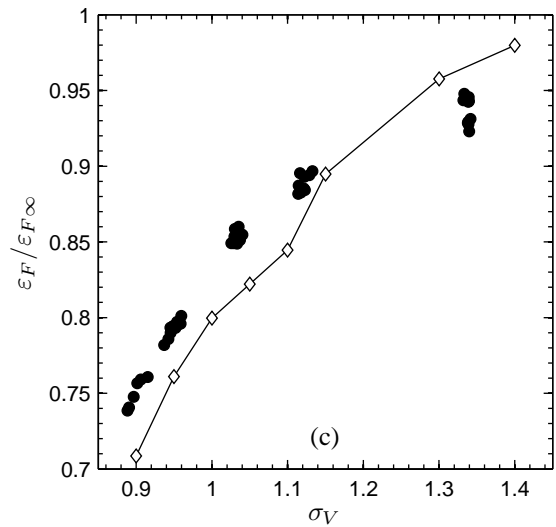
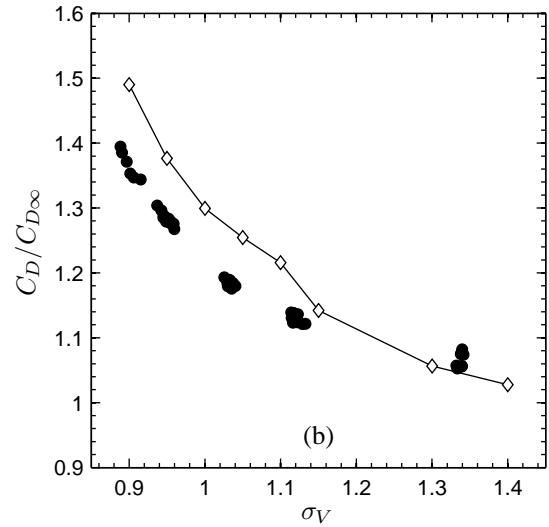
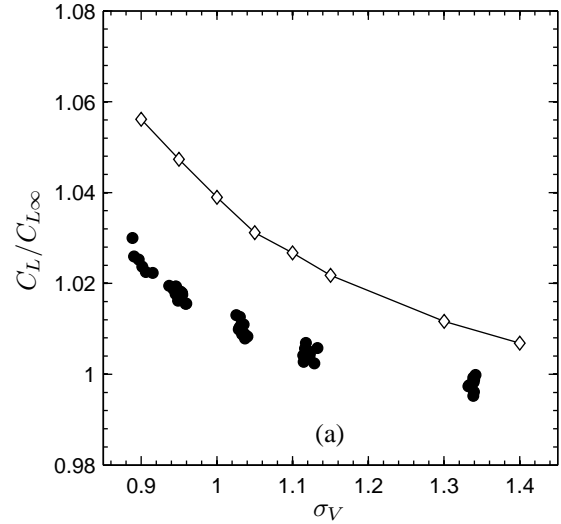


Figure 5: Comparison between the numerical results (\diamond) and the experimental results (\bullet) of lift coefficient (a), drag coefficients (b) and lift-to-drag ratio (c) of the 3D hydrofoil, section NACA0010, $\alpha = 7^\circ$; the subscript ∞ refers to non-cavitating condition

steady state flow condition. The cavitation numbers in this section are defined with respected to the advanced velocity

V_a of the propeller, $\sigma_V = (P_{ref} - P_V) / (\frac{1}{2}\rho V_a^2)$. In addition, since the pressure distribution on the blade tip sections is complex and related to the tip vortex cavitation, the partial sheet cavitation model is not applied on these sections.

4.1 Steady State Flow Condition

A marine propeller has been simulated with several cavitation numbers. The effect of the partial sheet cavitation on thrust coefficient K_T and torque coefficient K_Q as well as on propeller efficiency η is shown in figure 6. Like in the hydrofoil case, the thrust and torque coefficient increase when the cavitation number decreases.

However, only little effects are observed even when the cavity length reaches 3/4 of chord length in some sections near the blade tip as shown in figure 7. Furthermore, the propeller efficiency hardly decreases. These little effects are expected since the propeller hydrodynamic forces are originated from the section lift and the load distribution is not concentrated in the blade tip zone.

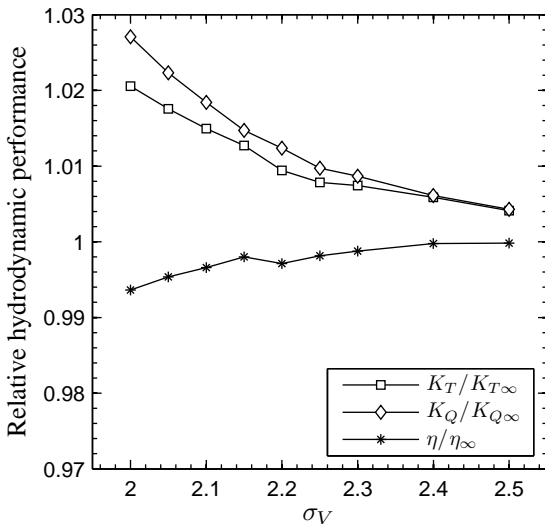


Figure 6: Effect of partial sheet cavitation on thrust, torque and efficiency of a marine propeller; the subscript ∞ refers to non-cavitating condition

4.2 Unsteady State Flow Condition

Some numerical simulations using the cavitation model in unsteady state flow condition have already been presented in Phoemsapthawee et al. (2008b). This last presentation was more focused and detailed on the hydrofoil simulations than on the propeller simulations. This time, a detailed numerical simulation of marine propeller in hydrostatic pressure field is presented.

The hydrostatic pressure makes the cavitation number to vary with depth. The simulation is set to have the variation of cavitation number as shown in figure 8. A snapshot of the obtained cavitating propeller is presented in figure 9. The cavity appears and increases in volume when the propeller blades approach to the free surface. Also as expected, the cavity decreases in volume and disappears

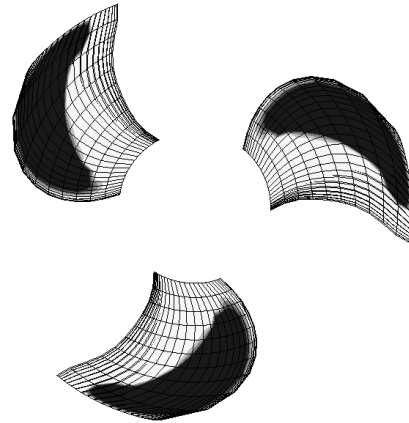


Figure 7: Cavity planform of a marine propeller in steady state flow condition, $\sigma_V = 2.0$

when the propeller blades move away from the free surface. The appearance and disappearance of the cavity makes the blade thrust and the blade torque coefficient to vary. The variation of thrust and torque coefficient of each propeller blade is presented in figure 10. There are some numerical noise in the numerical results. The assumption that the cavity does not depend on the previous time-step cavity shape might not be really appropriate and cause some numerical noise. However, the time-average results look reasonable. An example of pressure coefficient distribution on the section $r/R = 0.7$ ($R =$ propeller radius) when the blade is in the upper position (figure 9) is presented in figure 11.

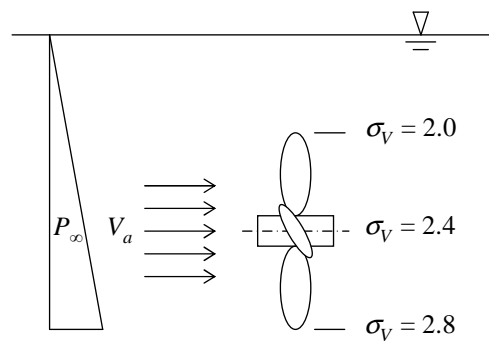


Figure 8: Configuration of the propeller simulation in hydrostatic pressure field

Like in the steady state flow case, the partial sheet cavitation has little effects on hydrodynamic forces. Nevertheless, this variation of hydrodynamic forces may combine with other unsteady hydrodynamic forces and may cause the ship vibration as well as the fatigue on propeller shaft and propeller blades.

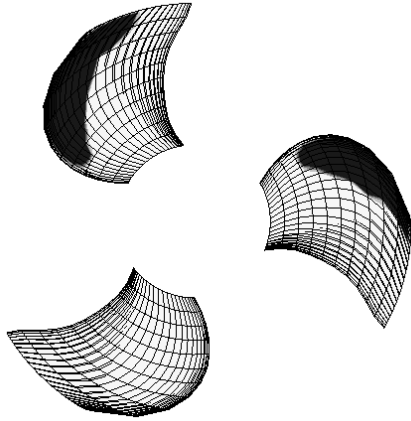


Figure 9: Partial sheet cavitation simulation on a marine propeller working in hydrostatic pressure field

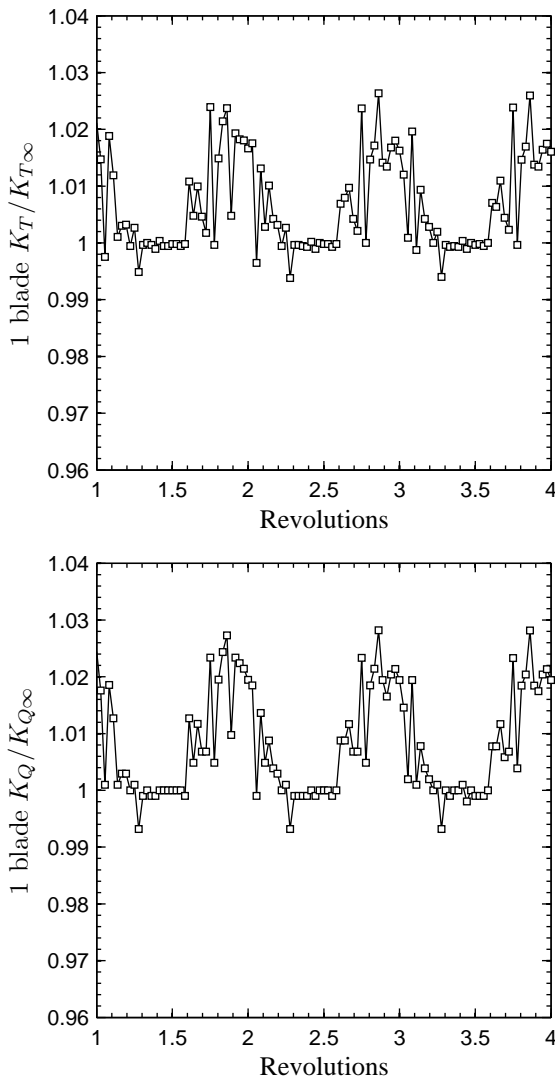


Figure 10: Variation of blade thrust and torque coefficient of the simulated marine propeller in hydrostatic pressure field; the subscript ∞ refers to non-cavitating condition

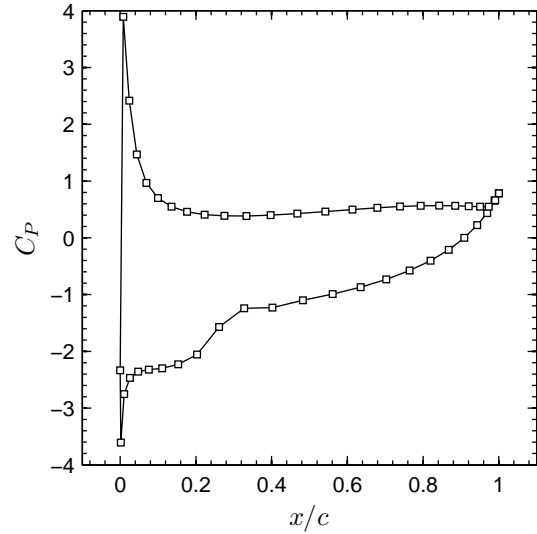


Figure 11: Pressure coefficient distribution on the section $r/R = 0.7$

5 CONCLUSION

A partial sheet cavitation model has been developed and implemented within a 3D BEM code to estimate the hydrodynamics forces and performance of a propeller working in an unsteady flow environment. In the previous works, the first stages of validation which consist in comparing a 2D computed pressure coefficient distribution and a 3D computed cavity length distribution with experimental data and other numerical simulations results was reported. In this paper, the last stage of validation in steady state flow condition is reported. It consists in comparing the computed hydrodynamic forces of a 3D hydrofoil with measured data.

Though the model so far can simulate only the partial sheet cavitation and the partial sheet cavitation has little effects on propeller hydrodynamic forces, the model has some advantages. The model can be used to find the limit where the partial sheet cavitation becomes the supercavitation. Furthermore, in spite of some noise in the numerical results, the model allows for fast unsteady state flow simulations.

ACKNOWLEDGEMENT

This work is supported by the Délégation Générale pour l'Armement. The authors wish to thank the BSHC (www.bshc.bg) for its kind cooperation, especially Mr. Valeri DIMITROV and Mrs. Anna STANEVA.

REFERENCES

- Balhan, I. (1951). Metingen aan enige bij scheepsschroeven gebruikelijke profielen in vlakke stroming met en zonder cavitatie. *Uitgave van het Nederlandsch Scheepsbouwkundig Proefstation te Wageningen*. Publicatie No.99.
- Brewer, W. and Kinnas, S. (1997). Experiment and viscous flow analysis on a partially cavitating hydrofoil. *Journal of Ship Research*, 41:161–171.

- Briançon-Marjolet, L. and Merle, L. (1999). Modélisation de la cavitation. Revue Scientifique et Technique de la Défense, 43:109–114. Bassin d'Essais des Carènes.
- Carlton, J. (2007). Marine propellers and propulsion. -2nd ed. ISBN: 978-07506-8150-6.
- Farhat, M., Guennoun, F., and Avellan, F. (2002). The leading edge cavitation dynamics. Proceeding of ASME: Fluids Engineering Division Summer Meeting. Montreal, Quebec.
- Franc, J. (1986). Etude physique d'écoulements cavitants. Thèse de Docteur d'Etat ès Sciences. Université de Grenoble.
- Hoeijmakers, H. (1992). Panel methods for aerodynamic analysis and design. AGARD Report, 783:5.1–5.47.
- Kinnas, S. and Fine, N. (1993). A numerical nonlinear analysis of the flow around two- and three- dimensional partially cavitating hydrofoils. Journal of Fluid Mechanics, 254:151–181.
- Krishnaswamy, P., Andersen, P., and Kinnas, S. (2001). Re-entrant jet modelling for partially cavitating two-dimensional hydrofoils. CAV2001 4th International Symposium on Cavitation. Pasadena, California.
- Laurens, J. (1993). Couplage code de calcul fluide parfait, code de calcul couche limite 3d. Rapport DCN/Bassin d'Essais des Carènes. Etude 2524 pièce 3.
- Lee, H. and Kinnas, S. (2004). Application of a boundary element method in the prediction of unsteady blade sheet and developed tip vortex cavitation on marine propellers. Journal of Ship Research, 48:15–30.
- Leroux, J. (2003). Etude expérimentale en tunnel hydrodynamique des instabilités de la cavitation par poche sur hydrofoil par la mesure spatio-temporelle du champ de pression pariétal. Thèse de Doctorat. Ecole Centrale de Nantes et Université de Nantes.
- Leroux, J., Astolfi, J., and Billard, J. (2003). Etude expérimentale des instationnarités et des instabilités des poches de cavitation. Acte des 9èmes Journées de l'Hydrodynamique. Poitiers, France.
- Peallat, J. and Pellone, C. (1996). Experimental validation of two- and three- dimensional numerical analysis of partially cavitating hydrofoils. Journal of Ship Research, 40:211–223.
- Phoemsapthawee, S., Leroux, J., Laurens, J., and Deniset, F. (2008a). Développement et validation d'un modèle de cavitation à poche sur hydrofoil et pale d'hélice. European Journal of Environmental and Civil Engineering, 12(5):509–521.
- Phoemsapthawee, S., Leroux, J., Laurens, J., and Deniset, F. (2008b). Partial sheet cavitation simulation on marine propeller in unsteady flow. Proceeding of the 8th International Conference on HydroDynamics, pages 163–170. Nantes, France.
- Rowe, A. and Blottiaux, O. (1993). Aspects of modelling partially cavitating flows. Journal of Ship Research, 37:34–48.
- Salvator, F. and Esposito, P. (2001). An improved boundary element analysis of cavitating three-dimensional hydrofoils. CAV2001 4th International Symposium on Cavitation. Pasadena, California.
- Vaz, G., Bosschers, J., and DeCompos, J. (2003). Two-dimensional modelling of partial cavitation with bem, analysis of several models. CAV2003 5th International Symposium on Cavitation. Osaka, Japan.
- Yamaguchi, H. and Kato, H. (1983). On application of nonlinear cavity flow theory to thick foil sections. Proceeding of the 2nd International Conference on Cavitation, IMechE C209/83:167–174. Edinburgh, Great Britain.